



Improved source parameter constraints for five undersea earthquakes from north component of GRACE gravity and gravity gradient change measurements



Chunli Dai^{a,*}, C.K. Shum^{a,d}, Junyi Guo^a, Kun Shang^a, Byron Tapley^b, Rongjiang Wang^c

^a Division of Geodetic Science, School of Earth Sciences, The Ohio State University, Columbus, OH, USA

^b Center for Space Research, University of Texas at Austin, TX, USA

^c Physics of Earthquakes and Volcanoes, GFZ German Research Centre for Geosciences, Potsdam, Germany

^d State Key Laboratory of Geodesy and Earth's Dynamics, Institute of Geodesy and Geophysics, Chinese Academy of Sciences, Wuhan 430077, China

ARTICLE INFO

Article history:

Received 28 September 2015

Received in revised form 5 March 2016

Accepted 12 March 2016

Available online xxx

Editor: P. Shearer

Keywords:

GRACE
north component
earthquakes
fault parameters

ABSTRACT

The innovative processing of Gravity Recovery And Climate Experiment (GRACE) data using only the north component of gravity change and its corresponding gravity gradient changes allows the enhancement of the spatial resolution for coseismic deformation signals. Here, we report the study of five undersea earthquakes using this technique: the 2004 Sumatra–Andaman earthquake, the 2007 Bengkulu earthquake, the 2010 Maule, Chile earthquake, the 2011 Tohoku earthquake, and the 2012 Indian Ocean earthquakes. By using the high spherical harmonic degree (up to degree 96) data products and the associated GRACE data processing techniques, the retrieved north component of gravity change is up to $-34 \pm 1.4 \mu\text{Gal}$ for the 2004 Sumatra–Andaman earthquake, which illustrates by far the highest amplitude of the coseismic signal retrieved from satellite gravimetry among previous studies. We creatively apply the localized spectral analysis as an efficient method to empirically determine the practical spherical harmonic truncation degree. By combining least squares adjustment with the simulated annealing algorithm, point source parameters are estimated, which demonstrates the unique constraint on source model from GRACE data compared to other data sources. For the 2004 Sumatra–Andaman earthquake, GRACE data produce a shallower centroid depth (9.1 km), as compared to the depth (28.3 km) from GPS data. For the 2011 Tohoku earthquake, the GRACE-estimated centroid location is southwest of the GPS/seismic solutions, and the slip orientation is about 10° clockwise from the published GPS/seismic slip models. We concluded that these differences demonstrate the additional and critical offshore constraint by GRACE on source parameters, as compared to GPS/seismic data.

© 2016 Elsevier B.V. All rights reserved.

1. Introduction

The quantification of large undersea earthquakes, including their sizes, location, geometry and orientation of the faults, is critical for improving our understanding of fault mechanisms, and for applications in tsunami warning. As pointed out by Geist et al. (2007), the centroid location and seismic moment are the most essential parameters (Meng et al., 2012; Tanioka and Satake, 1996) for tsunami forecast and hazard assessment models; while other first-order source parameters such as dip, fault length and width also affect the tsunami wave field (Geist et al., 2007). Besides seismic data and GPS data, which are traditionally used for studying focal mechanisms, other data sets including the Interferometric

Synthetic Aperture Radar (InSAR) data, tsunami data, and repeated airborne LiDAR data, have also been used. However, there are limitations for each type of data set on estimating the source parameters of undersea earthquakes.

Seismological methods have difficulty in estimating source parameters in some instances, e.g., seismic moment for ruptures with long duration due to the overlap of interfering arrivals (Chlieh et al., 2007; Lay et al., 2005), and seismic wave data are also inadequate for detecting slow or aseismic slip and postseismic slip (Chlieh et al., 2007; Han et al., 2013). One example for a long duration, slow rupture is the 2004 Sumatra–Andaman earthquake (Banerjee et al., 2005; Lay et al., 2005; Park et al., 2005), which also had large magnitude of afterslip (Chlieh et al., 2007). Lay et al. (2010) indicate that seismic inversions are sensitive to wave-form types and the frequency band, which is shown by the fact that different slip models are obtained from seismic waves with

* Corresponding author.

E-mail address: dai.56@buckeyemail.osu.edu (C. Dai).

different frequency bands. In addition, since seismic inversions are highly dependent on the velocity structure, they have instabilities for shallow ruptures (Lay et al., 2011).

Although geodetic measurements, such as GPS data, have the potential to overcome the inadequacy of seismological data in detecting slow/aseismic slip, they are limited by the spatial distribution of their ground-based sites. Particularly, for undersea earthquakes, although more ocean-bottom measurements are available, GPS stations are mostly located at one side of the fault area, thus providing limited constraints on source parameters (Chlieh et al., 2007; Lay et al., 2011; Wei et al., 2012). For example, Chlieh et al. (2007) and Wei et al. (2012) showed that inland static GPS data are quite insensitive to shallow ruptures and resolutions of inverted slip models decrease rapidly away from the coast.

The twin-satellite Gravity Recovery And Climate Experiment (GRACE) mission (Tapley et al., 2004) has been producing temporal global gravity field observations with monthly sampling rate and a spatial resolution up to spherical harmonic degree 60. The GRACE data have revolutionized our understanding of Earth's mass redistribution, including terrestrial hydrologic water balance, ocean mass variations and sea level rise, and ice-sheet and glacier ablation, and their possible links with anthropogenic climate change. As one of such mass redistribution processes, earthquakes trigger crustal/mantle dilation or compression and surface uplift or subsidence, causing permanent change in Earth's gravity field. By surveying right above the rupture region over the ocean, although with a coarse spatial and temporal resolution, GRACE data have been demonstrated to have the feasibility to complement other data for detecting and constraining focal mechanisms of large undersea earthquakes, since GRACE data have a better spatial coverage as compared to GPS data, and have better capability to detect aseismic slip as compared to seismic data. Several large earthquakes have been detected in GRACE data and analyzed in contemporary studies, including the 2004 Sumatra–Andaman earthquake (e.g., Han et al., 2006; Wang et al., 2012c), 2010 Maule, Chile earthquake (e.g., Han et al., 2010; Heki and Matsuo, 2010; Wang et al., 2012a), and the 2011 Tohoku earthquake (e.g., Cambiotti and Sabadini, 2012; Dai et al., 2014; Han et al., 2011, 2013; Li and Shen, 2015; Matsuo and Heki, 2011; Wang et al., 2012b). Moreover, GRACE has also shown its unique contribution to the detection of postseismic gravity signals (Han et al., 2014; Panet et al., 2010; Tanaka and Heki, 2014).

Recent studies explored different data processing methods to better retrieve co- and postseismic gravity change signal from GRACE data. Wang et al. (2012c) showed a spatial resolution enhancement by using the inferred gravity gradient changes computed from GRACE temporal gravity field solutions, for the 2004 Sumatra–Andaman earthquake. To optimize the spatial and temporal resolution, Han et al. (2011) directly exploited the signal of the 2011 Tohoku earthquake in the change of inter-satellite K-band range (KBR) rate. Wang et al. (2012a, 2012b) for the first time utilized the Slepian functions (Simons et al., 2006) to analyze GRACE-observed gravity changes aiming at the spatial resolution enhancement of the coseismic signals. The same techniques are also applied for the source parameters inversion by Cambiotti and Sabadini (2012). Furthermore, an innovative approach of using only the north component of gravity change (Dai et al., 2014), the corresponding gravity gradient change, e.g., T_{xx} and T_{xz} (x , z refers to north and up directions, respectively) change by Wang et al. (2012c), T_{xz} change by Li and Shen (2011), are found to substantially avoid the correlated errors in the GRACE temporal gravity field solution, with no decorrelation nor spatial filtering needed, leading to improved spatial resolution at the full wavelength corresponding to the highest spherical harmonic degree of GRACE data.

The inversion for several source parameters, such as the seismic moment, dip angle and rake angle, based on normal mode

formulation assuming point dislocation were demonstrated for the 2011 Tohoku earthquake (Han et al., 2011). Wang et al. (2012a, 2012b) adopted the Markov Chain Monte Carlo algorithm to invert for fault length and width of the 2010 Chilean Maule and the 2011 Tohoku earthquakes, based on a finite fault model assuming uniform slip. Cambiotti and Sabadini (2013) presented an estimation of all fault parameters (centroid location and moment tensor) for a point source using GRACE data. Han et al. (2013) solved for the seismic moment tensors of multiple centroids, but with locations fixed, based on the normal mode formulation for a number of large earthquakes over the last decade using GRACE data. Dai et al. (2014) further solved for the centroid location, seismic moment, fault width, and slip rake angle based on finite fault model using simulated annealing algorithm, and found that GRACE data are especially effective in constraining centroid location and slip orientation.

In this paper, the new approach of GRACE data processing using only the *north* component of gravity change and the corresponding gravity gradient change (Dai et al., 2014) is adopted to detect the coseismic signal for five recent large undersea earthquakes using several different GRACE products, including particularly the high degree (up to degree 96) CSR RL05 data. By using the linear algorithm of gravity and gravity gradient change with respect to the double-couple moment tensor, the point source parameters are estimated through a least squares adjustment combined with the simulated annealing algorithm. From the improved GRACE data processing method, the high degree (up to degree 96) data products, and the new inversion scheme, we solve for the point source parameters for the 2004 Sumatra–Andaman (M_w 9.2) earthquake, the 2011 Tohoku (M_w 9.0) earthquake, the 2010 Maule, Chile (M_w 8.8) earthquake, the 2012 Indian Ocean (M_w 8.6 and M_w 8.2) earthquakes, and the 2007 Bengkulu (M_w 8.5) earthquake. The results show the resolving power of GRACE data on slip orientation, and centroid location and depth.

2. Improved GRACE data processing

This work is based on the GRACE data processing method of using only the *north* component of gravity and gravity gradient changes developed in Dai et al. (2014). To enhance spatial resolution, we further advance this approach by applying the localized spectral analysis as an efficient method to determine the practical spherical harmonic truncation degree from high degree L2 products. As an example, this localized spectral analysis suggests that only the degrees less than 70 from the high degree (up to 96) CSR L2 Release 05 (RL05) monthly geopotential solutions contain reliable seismic signal for the 2011 Tohoku earthquake as shown in the following paragraph.

The localized spectra analysis (Wieczorek and Simons, 2005) is used as an efficient method to justify the choice of practical truncation degree. Dai et al. (2014) show the application of this localized spectral analysis in the way of evaluating the signal and noise level of each component of gravity and gravity gradient as function of spherical harmonic degree. Here we compute the localized degree variance, and the results are shown in Fig. 1. Where, the north, east, and down components of the gravity disturbance are denoted by g_N , g_E and g_D , and the north components of gravity gradient disturbances are denoted by T_{xx} , T_{xy} and T_{xz} (x , y , z , is north, west, up direction). The coseismic signal is estimated by fitting the GRACE-observed gravity and gravity gradient time series on a regular grid with a model composed of a Heaviside step function, a linear trend and three periodicities (equation A4, Fig. S1). We can see that the GRACE-observed g_N change (Fig. 1a) agrees well with the model prediction up until around degree 70, with slightly larger amplitude; while, the degree variance for GRACE-observed g_E and g_D change (Fig. 1a) increases sharply starting

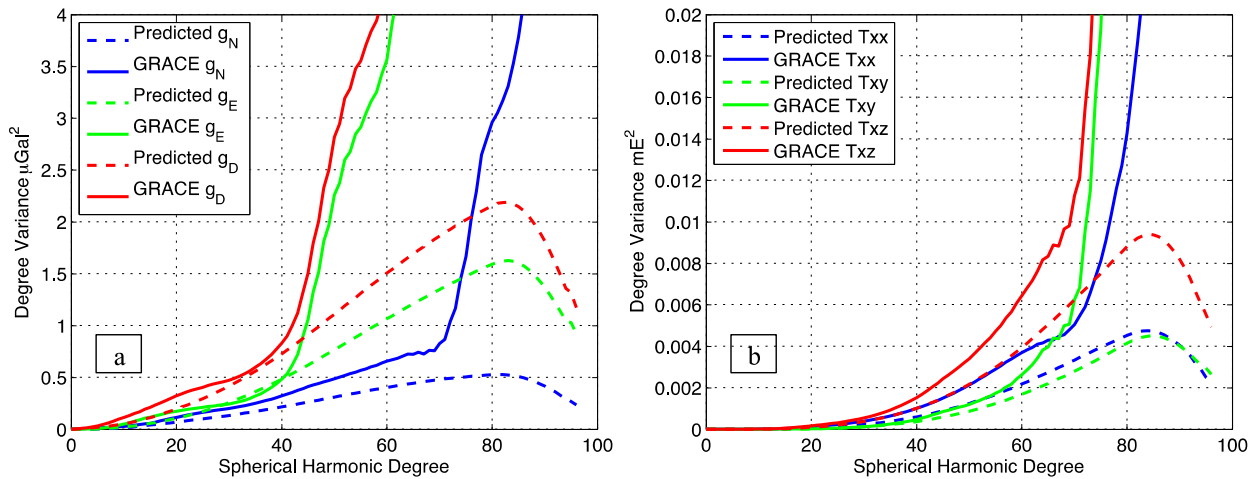


Fig. 1. Comparison between GRACE-observed and model-predicted gravity and gravity gradient change in the spectral domain for the 2011 Tohoku earthquake. The localized degree variance as a function of spherical harmonic degree is shown for the observed and model-predicted g_N , g_E , g_D change (a), and T_{xx} , T_{xy} , T_{xz} change (b). The GRACE-observed gravity and gravity gradient change is computed from the CSR RL05 NMAX 96 product up to maximum degree 96. The coseismic slip model by Wei et al. (2012) and the postseismic slip model for March 2011 by Ozawa et al. (2011) are used to calculate the model prediction using the forward modeling procedure in Dai et al. (2014).

from degrees at around 40, indicating that degrees higher than that are dominated by noise. This demonstrates that north component of gravity change contains reliable signal up to much higher degree than the east and down components of gravity change. Furthermore, as shown in Fig. 1a, the degree variance for g_N change keeps in good agreement with the model prediction until around degree 70, but above degree 70, the GRACE data is much higher than the model prediction, which we interpret as noise. Based on this, we choose to discard the spherical harmonic coefficients above degree 70 and compute the gravity and gravity gradient change (Fig. 1b) only up to degree 70, which will lead to good signal-to-noise ratio (in spatial domain as well).

Based on the localized spectral analysis, GRACE-observed and model-predicted north component of gravity and gravity gradient changes are compared for degrees up to 70, which is by now the highest degree of coseismic signal achievable by GRACE. As shown in Fig. S2, the spatial pattern of GRACE-derived gravity and gravity gradient change is evident and agrees well with the model prediction. For example, the GRACE-observed g_N change reaches up to $-24.0 \pm 3.9 \mu\text{Gal}$ at 140.2°E 36.85°N (Fig. S2a, Fig. S1b), with the magnitude slightly greater than the model prediction, $-18.5 \mu\text{Gal}$. And the T_{xx} change (Fig. S2b) also has good consistency with the model prediction (Fig. S2f).

3. Source parameters inversion method

For seismic source model inversion, instead of solving for the finite fault model as shown in previous studies (Cambiotti and Sabadini, 2012; Wang et al., 2012a, 2012b; Dai et al., 2014), here we choose to directly solve for the moment tensor of a point source as presented in (Han et al., 2011, 2013; Cambiotti and Sabadini, 2013). This simple point-source moment tensor is adopted to represent the source model mainly because of the linear relationship between the coseismic gravity and gravity gradient change and the double-couple moment tensor elements, as well as the lower sensitivity of GRACE to the extension of finite fault area (Cambiotti and Sabadini, 2012; Dai et al., 2014). The seismic moment tensor can be straightforwardly resolved using least-squares adjustment (see details in supplementary materials). The simulated annealing algorithm (Kirkpatrick et al., 1983) is further used to solve for the centroid depth and location, because of the non-linear relationship between centroid location and coseismic gravity change.

4. Inversion for source parameters

GRACE data have already been shown to provide good constraint on seismic moment, centroid depth (Han et al., 2011, 2013), centroid location (Cambiotti and Sabadini, 2013; Dai et al., 2014), and slip orientation (Dai et al., 2014). The sensitivity study by comparing the residuals for the inverted source parameters at various depths (Fig. S3) further shows that GRACE data are able to detect the source depth. Here we present the inversion for all source parameters of a point source including the centroid location and depth together with its seismic moment tensor, using the improved-processed high-degree GRACE data products.

4.1. The 2004 Sumatra–Andaman and 2005 Nias earthquakes

The 26 December 2004 Sumatra–Andaman (M_w 9.2) megathrust earthquake was the largest earthquake in the last 50 yrs, and it ruptured about 1500 km of the subduction zone along the India–Burma plate boundary. Three months later, the 28 March 2005 Nias (M_w 8.6) earthquake ruptured about 300 km at the adjacent Australia–Sunda plate boundary. In this study, we evaluate the cumulative coseismic slip deformation for the two events from GRACE data, considering the short time difference between these two earthquakes. We first compare GRACE measurements with that predicted from the cumulative coseismic slip models (Chlieh et al., 2007; Konca et al., 2007), then we solve for the fault parameters using GRACE-derived gravity and gravity gradient change.

For these two megathrust earthquakes, the gravity and gravity gradient change are estimated from the high degree monthly solutions (up to degree 90) of GFZ RL05a NMAX 90 product. CSR RL05 NMAX 96 product are also used to study the coseismic gravity change, but shows a worse model-data misfit compared to GFZ RL05a product. Two more large earthquakes occurred in Sumatra and its nearby region in the last decade, including the 2012 Indian Ocean earthquakes (M_w 8.6 and M_w 8.2), and the 2007 Bengkulu earthquake (M_w 8.5). Considering the overlap of the fault area, three coseismic jumps at 26 December 2004, 11 April 2012, and 12 September 2007 are estimated jointly using three Heaviside step functions corresponding to these three earthquakes and a linear trend and three periodicities to fit the GRACE-observed gravity and gravity gradient time series (Fig. S1a) at each grid point. For the 2004 Sumatra–Andaman earthquake, although the coseismic signal is estimated at the epoch 26 December 2014, we con-

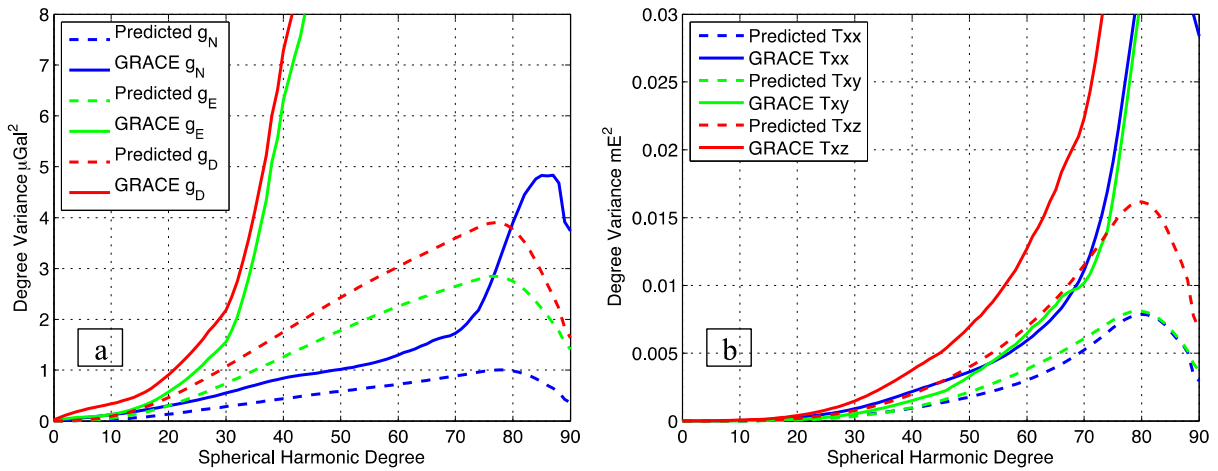


Fig. 2. Comparison in the spectral domain up to degree 90 from GFZ RL05a product. The coseismic slip distribution model (http://www.tectonics.caltech.edu/slip_history/2004_sumatra/update1/slipAceh_BSSA2007) given by Chlieh et al. (2007) for the 2004 Sumatra–Andaman earthquake, and the coseismic slip distribution model (http://www.tectonics.caltech.edu/slip_history/2005_sumatra/update2/static_out) by Konca et al. (2007) for the 2005 Nias earthquake, are used for the model prediction. Other descriptions are the same as in Fig. 1.

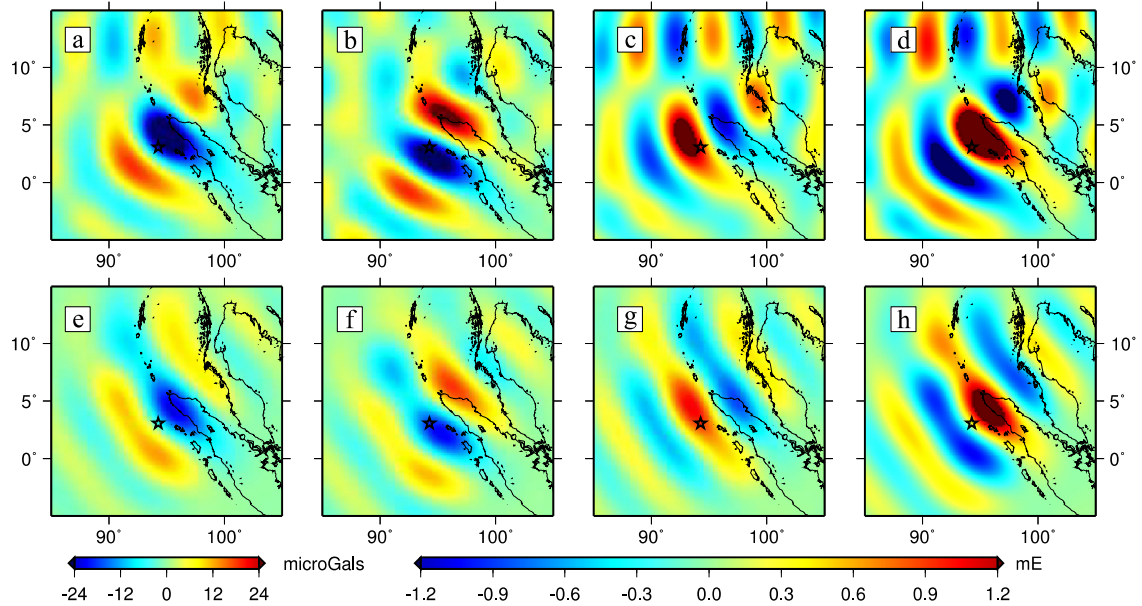


Fig. 3. Comparison of GRACE-produced and model-predicted gravity and gravity gradient change up to degree 65 from GFZ RL05a product for the 2004 Sumatra–Andaman earthquake. (a)–(d): GRACE-observed g_N (a), T_{xx} (b), T_{xy} (c), T_{xz} (d) change, respectively. (e)–(h): model-predicted g_N (e), T_{xx} (f), T_{xy} (g), T_{xz} (h) change, respectively. The black star is the GCMT (Global Centroid Moment Tensor Project) centroid (94.26°E, 3.09°N).

consider the jump as the cumulative signal for the two earthquakes three months apart, since the number of data after the two events greatly outweighs the three months of data from January to March 2005.

The localized spectra analysis is carried out for GRACE-observed and model-predicted gravity and gravity gradient change (Fig. 2). We can see that the GRACE-observed g_N change agrees well with the model prediction up until around degree 70, although the amplitude is slightly larger than the model prediction. Similarly, for the gravity gradient change, GRACE-observed value is larger than the model prediction but has good agreement until around degree 65. Above degree 65, the GRACE data is much higher than the model prediction, which we interpret as noise. Using the new application of this localized spectra analysis to justify the choice of practical truncation degree, and based on additional comparison in spatial domain, we choose to discard the spherical harmonic coefficients above degree 65.

Hence, GFZ RL05a solutions are truncated to degree 65 to retrieve g_N , T_{xx} , T_{xy} and T_{xz} time series. As shown in Fig. S1a, the earthquakes cause the g_N significantly decreasing by about $34 \pm 1.4 \mu\text{Gal}$, which is by far the highest coseismic signal achievable by innovative GRACE data processing. The overall positive–negative–positive pattern for the GRACE-derived g_N change (Fig. 3a) over the Aceh region and surrounding ocean is consistent with the slip model prediction (Fig. 3e). The maximum g_N change ($-34 \pm 1.4 \mu\text{Gal}$) is almost twice of the model prediction at the same point, $-19.4 \mu\text{Gal}$. GRACE-derived g_N change is larger than the model prediction mainly due to the small shear modulus value (30 GPa) applied in our forward model prediction, which underestimates the moment by about half. Coinciding with g_N change, the GRACE-derived gravity gradient change (Fig. 3b–d), T_{xx} , T_{xy} , T_{xz} also matches well with the model prediction.

For our source parameters inversion, we adopt the same earth structure model (Chlieh et al., 2007) as the one

used for the forward model prediction (Fig. 3) to reduce the bias caused by structural differences. The GRACE-estimated location (red star in Fig. 4) is remarkably close to the GCMT solution (black star, <http://www.globalcmt.org/>). It is west of the USGS CMT (http://comcat.cr.usgs.gov/earthquakes/eventpage/official20041226005853450_30#scientific_summary, green beach ball), and south of the cumulative coseismic slip models (blue beach ball) (Chlieh et al., 2007; Konca et al., 2007). Poisson et al. (2011) demonstrated that the best model that reproduces the tsunami data among five published slip models is the slip model of Rhie et al. (2007), which has the peak slip at south of Nicobar Island, close to our centroid location.

Our estimated centroid depth (9.1 km) is much shallower than the depth (28.6 km) resolved using seismic data (GCMT and USGS CMT) and the depth (28.3 km) from geodetic data (Chlieh et al., 2007; Konca et al., 2007). The underestimation of slip at the updip direction and overestimation of slip at downdip direction (closer to measurements) from the checkerboard test (Chlieh et al., 2007), might explain the deeper centroid by geodetic data compared to our solution by GRACE data. In addition, the shallow sediments near trench are thought to accommodate relative plate motions aseismically (Lay et al., 2012). Hence, the afterslip, which releases about 35% of the coseismic moment (Chlieh et al., 2007), might occur at the shallow region, contributing toward a shallower centroid depth. Finally, the GRACE-solved location is closer to the trench (Fig. 4 bottom), which indicates a shallow source.

Our estimated centroid moment tensor, with a total moment of 6.09×10^{22} Nm, is the total of the coseismic slip of the 2004 Sumatra–Andaman earthquake, the afterslip and postseismic slip over the following three months, and coseismic slip of the 2005 Nias earthquake. The estimated moment, M_0 , is smaller than the published total moment (10.37×10^{22} Nm), which is the sum of the coseismic moment 6.93×10^{22} Nm, one-month postseismic moment 2.44×10^{22} Nm by (Chlieh et al., 2007), and the coseismic moment 1.0×10^{22} Nm (Konca et al., 2007) for the 2005 Nias earthquake. Dip angle is another important source parameter since the estimation of moment has a strong dependence on dip (Banerjee et al., 2005; Rhie et al., 2007; Han et al., 2011, 2013) for shallow thrust earthquakes. The sensitivity test by Rhie et al. (2007) shows the dip angle is not well resolved using the long-period teleseismic data and near-field GPS displacements. Our estimated dip angle, δ , is 32° (Table S1), larger than the mean value (14°) of cumulative coseismic slip models by Chlieh et al. (2007) and Konca et al. (2007). Based on the plate boundary geometry (Fig. 4 profile AA'), it seems that the GRACE-estimated dip angle is also larger than the slope angle of the subducting slab. One possible cause for our smaller seismic moment and larger dip angle might be the trade-off between these two parameters for shallow thrust earthquakes (Han et al., 2013), where the trade-off is revealed by their large correlation of 0.4 (Table S6, equation A2). This trade-off implies that the $M_0 \sin(2\delta)$ is better constrained than each of M_0 and dip individually (Han et al., 2011). As shown in the moment-dip comparison (Fig. S7), the GRACE-estimated solution is consistent with the cumulative slip model in terms of $M_0 \sin(2\delta)$. Our slip azimuth (Dai et al., 2014) is about 8° clockwise of the GCMT and USGS CMT solution, and 8° anticlockwise of the cumulative slip distribution models by Chlieh et al. (2007) and Konca et al. (2007). The correlation (Table S6) between strike and rake angle is strong, up to about one, which is consistent with the trade-off between these two angles as discussed in Han et al. (2011, 2013) and Dai et al. (2014), indicating that the slip azimuth is better constrained from GRACE data compared to the strike and rake angle individually for the small-dip thrust earthquakes. For these mega thrust earthquakes, although a single point source is only a simple approximation for the long rupture, it provides the critical prior information (the location, dip angle, strike angle) for the slip dis-

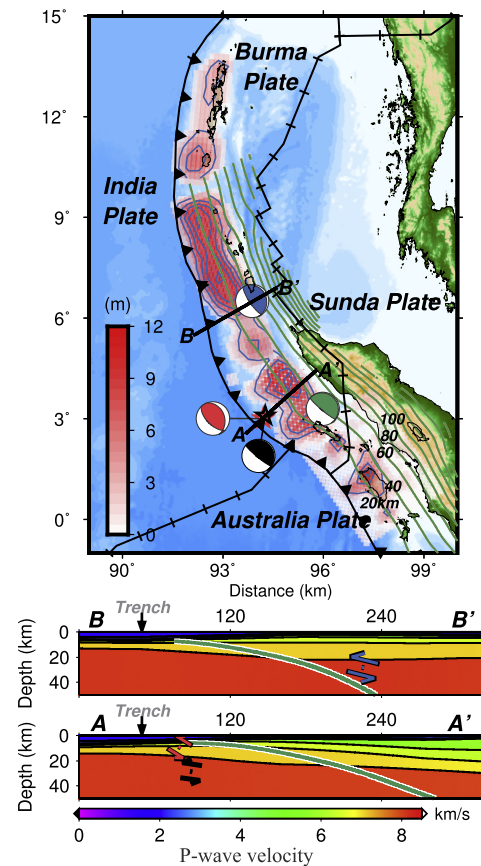


Fig. 4. Comparison of centroid moment tensor solutions. In **top** panel, the blue slip contours are for the cumulative slip distribution models (red 2D image) (Chlieh et al., 2007; Konca et al., 2007) on the fault plane. The red image along the India–Burma plate boundary is for the slip model by Chlieh et al. (2007) for the 2004 Sumatra–Andaman earthquake, and the red 2D map along the Australia–Sunda plate boundary is for the slip model (Konca et al., 2007) of the 2005 Nias earthquake. The blue beach ball represents the centroid location and moment tensor estimated from the cumulative slip distribution models, where the centroid moment tensor is computed using the summation of every moment tensor at each patch on the fault plane, and the centroid location and depth is computed using the weighted average of every patch's location, with the moment on each fault patch as the weight. The GCMT solution is denoted as the black beach ball, with location at the black star. Green beach ball represents USGS CMT solution and location. Red beach ball is CMT solution from GRACE GFZ RL05a data, with the location at the red star (94.20°E , 3.00°N , 9.1 km). The thick black line is the plate boundary (Bird, 2003), with black triangular representing the subduction zone. The green lines indicate the depth contours of the subducting slab at 20-km intervals from Slab1.0 model (Hayes et al., 2012) (<http://earthquake.usgs.gov/data/slab/>). The **bottom** two panels give the vertical profiles of the subducting slab and the crustal structure for profiles AA' and BB' as marked in the top panel. The crustal structure is interpolated from the CRUST 1.0 model (<http://igppweb.ucsd.edu/~gabi/rem.html>). The green curve denotes the subducting slab. Black lines are the interfaces between different layers, where the red layer with P-wave velocity of around 8 km/s denotes the mantle. The red, blue, and black arrows denote the centroids locations and dip angles for these red, blue, and black beach balls in the left panel, respectively, i.e., the red arrow is for GRACE solution (9 km depth, 32° dip), the blue arrow is for the cumulative slip distribution models (28 km depth, 14° dip), and the black arrow is for the GCMT solution (29 km depth, 8° dip). The GRACE-estimated depth is consistent with the shallow subducting slab near the Trench. (For interpretation of the references to color in this figure legend, the reader is referred to the web version of this article.)

tribution model inversion when using near-field GPS displacements or seismic data. In future studies, we will investigate the potential modeling error caused by using one single point source for the case of a long rupture.

4.2. The 2011 Tohoku earthquake

For the 11 March 2011 Tohoku earthquake (M_w 9.0), the GRACE-derived north component of gravity and gravity gradient

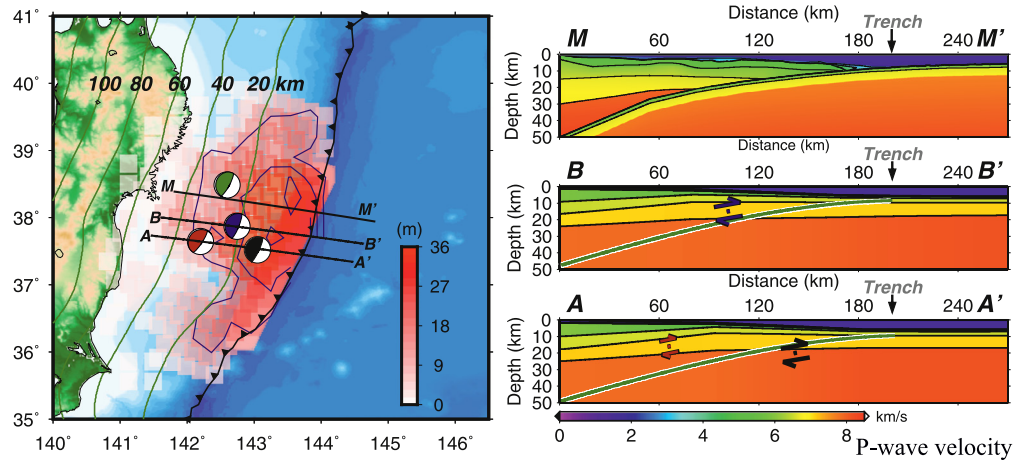


Fig. 5. Comparison of centroid moment tensor solutions for the 2011 Tohoku earthquake. In the **left** panel, the red image overlapped on the topography/bathymetry along the trench is for the cumulative coseismic and postseismic (March 2011) slip model (Wei et al., 2012; Ozawa et al., 2011), with contours represented by the blue lines and CMT denoted by the blue beach ball. Red beach ball is CMT solution from GRACE data (CSR RL05 NMAX 96 product), located at 142.2°E, 37.65°N, with depth as 16 km. The **right** three panels give the vertical profiles of the subducting slab and the crustal structure for the profiles MM' , BB' , and AA' , as shown in the left panel. The green curves in BB' and AA' denote the subducting slab. The MM' profile denotes the velocity structure at the Japan Trench deduced from a seismic experiment (Miura et al., 2005), showing details of the subducting slab, demonstrating consistent characteristics with the slab along the profile BB' from Slab1.0. Black lines are the interfaces between different layers, where the red layer with P-wave velocity of around 8 km/s denotes the mantle. The red, blue, and black arrows denote the centroid location and dip angles given by GRACE data (16 km depth, 12° dip), by the slip distribution model (18 km, 10° dip), and that by the GCMT solution (20 km depth, 10° dip). Other markings are the same as in Fig. 4. The GRACE-estimated dip angle (12°) (red arrow in AA') agrees well with the dip angle of the subducting slab. (For interpretation of the references to color in this figure legend, the reader is referred to the web version of this article.)

Table 1
The correlation between parameters.

	Strike	Dip	Rake	M_0	Strike	Dip	Rake	M_0	Strike	Dip	Rake	M_0
Strike	1	0.4	1	0	1	0	0.9	-0.2	1	0.2	0.2	0
Dip	0.4	1	0.2	0.1	0	1	-0.1	0.6	0.2	1	0.4	0
Rake	1	0.2	1	0.1	0.9	-0.1	1	-0.2	0.2	0.4	1	0
M_0	0	0.1	0.1	1	-0.2	0.6	-0.2	1	0	0	0	1

Left panel for the 2011 Tohoku earthquake, the **middle** panel for the 2010 Maule, Chile earthquake, and the **right** panel is for the 2012 Indian Ocean earthquakes. The correlation coefficient, which is calculated from the covariance and standard deviations of the estimated parameters (equation A2 in the supplementary material), evaluates the degree of linear relationship between variables.

change up to degree 70 from CSR RL05 NMAX 96 product as presented in Section 2 are used to solve for the centroid moment tensor of the earthquake source. The estimated centroid location and source parameters from this high degree L2 product are basically consistent with the finite fault parameters inverted using GRACE CSR RL05 NMAX 60 product (Dai et al., 2014). The location is at 142.2°E, 37.65°N (red beach ball in Fig. 5), which is only 13 km away from the centroid location determined by Dai et al. (2014). The consistency of the two solutions demonstrates the coherence of the two GRACE products, as well as the coherence of the finite fault modeling and the centroid moment tensor modeling. As discussed by Dai et al. (2014), the GRACE-estimated centroid location is almost parallel in latitude with the GCMT centroid, and it is close to the centroid latitude from GRACE data by Cambiotti and Sabadini (2013). As regards to its distance to the coast, GRACE-estimated centroid is between the location estimated by GPS data only (Ozawa et al., 2011) and the location (blue beach ball) estimated by the combined seismic waves data and on-land/offshore GPS data (Wei et al., 2012). The GRACE-estimated depth (16 km) indicates a shallow rupture, and agrees well with the centroid depth (18 km) by ruptured seismic data and GPS data (Wei et al., 2012), as well as the centroid depth (17 km) constrained by GRACE KBR data (Han et al., 2011) and that (16 km) by differently processed GRACE L2 data (Cambiotti and Sabadini, 2013).

The GRACE-estimated seismic moment, $(4.03 \pm 0.01) \times 10^{22}$ Nm, is slightly smaller than the published results (Han et al., 2011; Ozawa et al., 2011; Wei et al., 2012). The GRACE-estimated dip angle ($12 \pm 0.1^\circ$) agrees well with the published results, with difference less than 2° , especially agrees well with the dip angle of

the subducting slab (Fig. 5 right). Although the strike ($236 \pm 0.5^\circ$) and rake angles ($113 \pm 0.5^\circ$) are about 30° larger than those inverted from the finite fault model (Dai et al., 2014) that fixed the strike angle at 201° , considering the strong correlation between the strike and rake angle (Table 1 left), our slip azimuth (123°) is almost the same with the slip azimuth (124°) in Dai et al. (2014). This slip azimuth is consistent with the earlier conclusion that the GRACE-inverted slip direction is about 10° clockwise from that inverted by GPS and seismic waves data (Wei et al., 2012), but it is only about 3° clockwise from the USGS CMT slip direction. Furthermore, this clockwise rotation of the slip direction is validated by another satellite gravity gradiometry measurements – Gravity field and steady-state Ocean Circulation Explorer (GOCE) (Fuchs et al., 2013). One explanation for the clockwise 10° difference in the slip azimuth is that the observed onshore deformation by the GPS network is more sensitive to the deep fault slip close to coast but less sensitive to the shallow slip near the trench, while the GRACE-observed gravity data are most sensitive to the largest offshore shallow slip near the trench. Based on finite-fault inversions (Wang et al., 2013), there is an indication to a variable rake angle increasing with depth. Therefore the average slip azimuth angle estimated by GPS can be smaller than that by GRACE.

4.3. The 2010 Maule, Chile earthquake

The 27 February 2010 Maule, Chile (M_w 8.8) earthquake ruptured about 500 km along Nazca–South American plate boundary, with the Nazca oceanic crust subducting under the continent of the South American plate to the east direction. For the coseismic

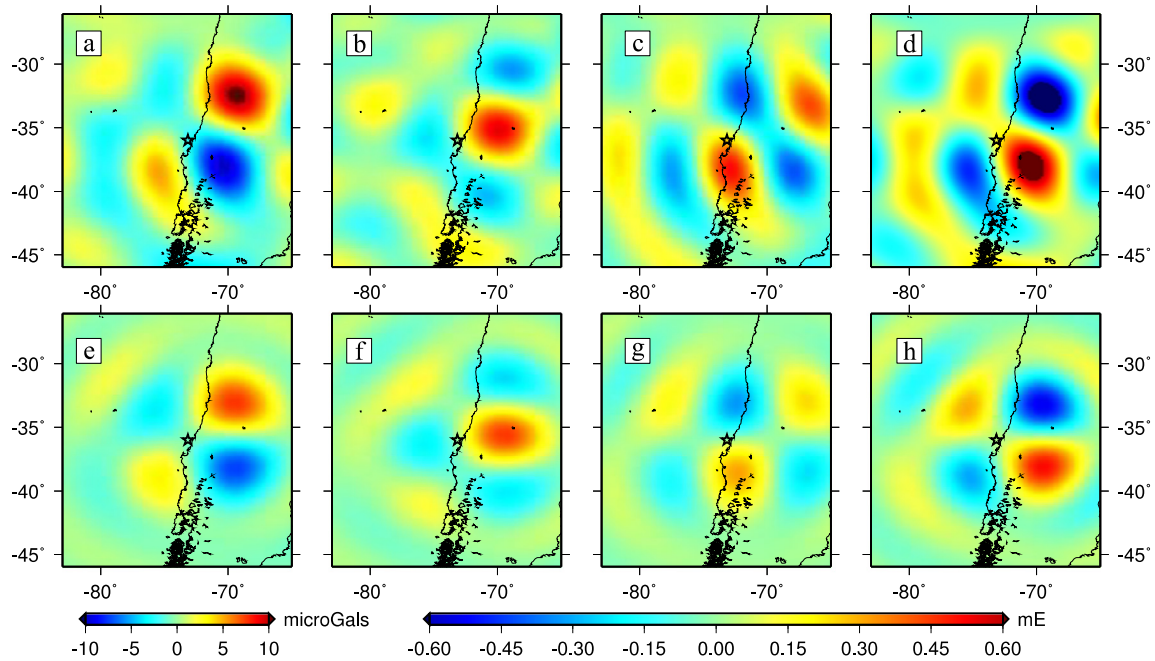


Fig. 6. Comparison of GRACE-produced and model-predicted gravity and gravity gradient change up to degree 60 from CSR RL05 product for the 2010 Maule, Chile earthquake. (a)–(d): GRACE-observed g_N (a), T_{xx} (b), T_{xy} (c), T_{xz} (d) change, respectively. (e)–(h): model-predicted g_N (e), T_{xx} (f), T_{xy} (g), T_{xz} (h) change, respectively. The model prediction is corresponding to the slip model in Hayes (2010) (<http://on.doi.gov/yVUCUQ>). The black star is the GCMT centroid (73.15°W, 35.98°S).

gravity change detection, although g_N change from GRACE contains reliable signal up to much higher degree than g_D change, the magnitude of coseismic g_N change can be smaller compared to g_D change depending on fault parameters. For example, for this east–west slip earthquake, the model-predicted g_N change is only about 40% of the g_D change up to degree 60. Nevertheless, GRACE-observed g_N change still shows its advantage on coseismic signal detection for this 2010 Maule, Chile earthquake as shown later.

The coseismic gravity and gravity gradient change up to degree 60 are retrieved using monthly solutions from CSR RL05 product. For the forward model prediction, we start from the USGS finite fault model by Hayes (2010), shown in red overlapped on top of the local topography/bathymetry in Fig. 7. The GRACE-observed g_N , T_{xx} , T_{xy} , T_{xz} change agrees with the model prediction with slightly larger magnitude in both spectral domain and spatial domain up to degree 60. For the GRACE-derived g_N change, the quadruple spatial pattern is consistent with the model prediction. The peak g_N change is $10.6 \pm 1.3 \mu\text{Gal}$ at 69.4°W 32.45°S as shown in Fig. S1c and Fig. 6a, slightly larger than the predicted value, $7.2 \mu\text{Gal}$. Even for this adverse case of east–west slip, the GRACE-derived g_N change still has slightly larger magnitude than the peak g_D change of $-8.0 \mu\text{Gal}$ from GRACE data (Wang et al., 2012a), due to the smoothing filter applied for g_D to reduce stripes. The north component of gravity gradient change (Fig. 6b–d) also match well with the model prediction, with peak value of T_{xz} as $-0.75 \pm 0.11 \text{ mE}$, slightly larger than its model prediction, -0.51 mE .

GRACE-solved centroid location (73.4°W , 35.2°S , red star in Fig. 7) using CSR RL05 product is northwest of the centroid solved by other data sets (Hayes, 2010; Vigny et al., 2011). For example, it is about 40 km north and 50 km west of the centroid location (blue beach ball) by Hayes (2010) from broadband seismic waves, and it is about 20 km west and 80 km north of the GCMT centroid (black beach ball). To check the uncertainty on solved source parameters caused by different GRACE L2 data processing, another two L2 products, the latest JPL RL05.1 and GFZ RL05a data products, are also used for the inversion. Both products are truncated at degree 50 to reduce the noise at high degrees. We can see that the GRACE-solved CMT locations by CSR RL05 and JPL RL05.1 prod-

ucts are almost identical to each other, which can be explained by the fact that the two data products are solved using similar background models and data processing strategies. While the GFZ RL05a product produce a location about 50 km north and 50 km east of that by the CSR RL05 product. The discrepancy on the locations by three data products may, to a certain extent, represent the uncertainty of the centroid location inverted from GRACE data. Nevertheless, for this earthquake, GFZ RL05a data product shows a relatively higher noise level on the gravity and gravity gradient change (figures not shown), which is also shown by its larger RMS (Root Mean Square) data-model differences (e.g. $1.0 \mu\text{Gal}$ for g_N) as compared to the value ($0.93 \mu\text{Gal}$ for g_N) by the JPL RL05.1 product, where the model is the GRACE-inverted CMT solution using each data product.

GRACE-estimated depth (20.7 km) by the three L2 data products are the same (Table S2), which indicates its small uncertainty. This GRACE-estimated depth is consistent with the published depths from geodetic data (Vigny et al., 2011; Pollitz et al., 2011), which show major slip locates at the shallow depth ($<25 \text{ km}$). It is also close to the depth from seismic waves data by GCMT. The shallow slip given by GRACE and GPS data is in consistency with the generation of a strong tsunami and the numerous aftershocks near the trench.

GRACE-resolved seismic moment, $(2.17\text{--}2.6) \times 10^{22} \text{ Nm}$, is close to the M_0 , $2.39 \times 10^{22} \text{ Nm}$, by Hayes (2010). But it's slightly larger than the M_0 , $(1.55\text{--}1.97) \times 10^{22} \text{ Nm}$, in Pollitz et al. (2011), and Vigny et al. (2011), as well as that by GCMT and USGS CMT. Nevertheless, GRACE-resolved dip angle ($25\text{--}26^\circ$) is about 8° larger than the average value (18°) of dip angle by seismic waves and that by geodetic data (Pollitz et al., 2011). It has been long known that there is a trade-off between seismic moment and dip angle for shallow thrust earthquakes (rake $\approx 90^\circ$) (Han et al., 2013). For this earthquake with rake angle (99°) close to 90° , this trade-off might play a role in the larger GRACE-inverted dip angle, where the coupling is also revealed by their large correlation of 0.6 (Table 1 middle). Moreover, the GRACE-estimated moment and dip are in accordance with the solution by Hayes (2010) in terms of $M_0 \sin(2\delta)$ (Fig. S7). The azimuth of slip direction from CSR RL05

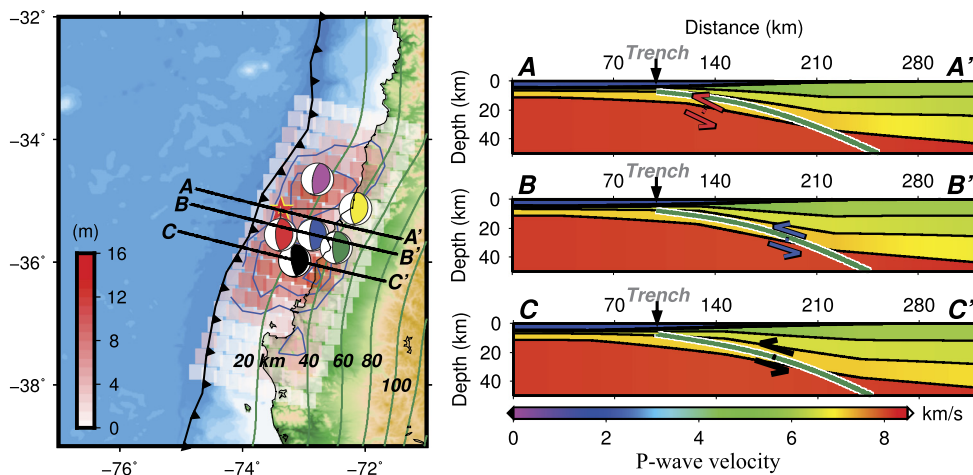


Fig. 7. Comparison of centroid moment tensor solutions for the 2010 Maule, Chile earthquake. In **left** panel, the red image overlapped on the topography/bathymetry along the Nazca/South American plate boundary is for the slip model by Hayes (2010), with contours represented by the blue lines and CMT denoted by the blue beach ball. Red beach ball is CMT solution from GRACE CSR RL05 product, located at 73.4°W, 35.2°S (red star), with depth as 20.7 km. Yellow star is the location (73.4°W, 35.1°S, 20.7 km) of CMT solution (yellow beach ball) from GRACE JPL RL05.1 product, which is almost overlapped by the red star since they are only about 4 km apart. Magenta beach ball is the CMT solution from GRACE GFZ RL05a data product, located at 72.8°W, 34.6°S, with depth as 20.7 km. USGS CMT (green beach ball) is from http://earthquake.usgs.gov/earthquakes/eqinthenews/2010/us2010tfan/neic_tfan_cmt.php. The **right** three panels give the vertical profiles of the subducting slab and the crustal structure for the profiles AA', BB', and CC', as shown in the left panel. The red, blue, and black arrows denote the centroid location and dip angles given by GRACE CSR RL05 data (21 km depth, 26° dip), by the slip distribution model (28 km, 18° dip), and that by the GCMT solution (23 km depth, 18° dip). Other markings are the same as in Fig. 4. (For interpretation of the references to color in this figure legend, the reader is referred to the web version of this article.)

and JPL RL05.1 products is close to that in Hayes (2010) and that by USGS CMT, while the slip azimuth from GFZ RL05a is about 10° different. As a trial, we also solve for the CMT parameters with location and depth fixed at the GCMT solution. By fixing the centroid location, the estimated slip azimuth is 13° anticlockwise of that in Hayes (2010), leading to a worse relative difference (equation A3), 59.5%, compared to the 53.9% from the SA inversion. This test shows that an inaccurate presumed location may affect the solution for the CMT parameters.

4.4. The 2012 Indian Ocean earthquakes

The 11 April 2012 Indian Ocean (M_w 8.6 and M_w 8.2) earthquakes ruptured within the Indian Oceanic plate near the India–Australia plate boundary off the west coast of northern Sumatra. The mainshock of M_w 8.6 is the largest strike-slip earthquake on record (Delescluse et al., 2012; Meng et al., 2012; Yue et al., 2012), and the aftershock occurred just two hours later with the magnitude of M_w 8.2. Because of its remote offshore location, the geodetic constraints on the static fault geometry are limited (Meng et al., 2012); thus only seismological data are used to invert for the focal mechanisms. Hence, GRACE data become an important source of independent constraint on the coseismic static deformation. Although the gravity change for vertical strike-slip earthquakes is expected to be small, we show that the coseismic gravity change from GRACE is still considerable, up to $-5.7 \pm 0.7 \mu\text{Gal}$ for g_N (Fig. S1d) and $0.26 \pm 0.03 \text{ mE}$ for T_{xx} .

Three products are used to estimate the coseismic gravity and gravity gradient change, including the OSU product generated by Shang et al. (2015) using the improved energy integral approach (Guo et al., 2015; Shang et al., 2015), the CSR RL05 NMAX 60 product and the GFZ RL05a NMAX 90 product. All solutions are truncated to degree 40 based on the localized spectral analysis and the signal's spatial pattern. The RMS of the difference between the GRACE-estimated g_N , T_{xx} , T_{xy} , T_{xz} and the model prediction are evaluated as shown in Table S3. It shows that GFZ RL05a gives the largest RMS difference, while the CSR RL05 and OSU product produce comparable and small RMS difference. Here, we choose to show the results from the CSR RL05 product.

Guided by the localized spectral comparison, we use only the north component of gravity and gravity gradient change up to degree 40 to study the coseismic signal. As shown in Fig. S4a, the GRACE-derived g_N change and gravity gradient change agree well with the cumulative slip model predictions (Yue et al., 2012) in spatial pattern and signal magnitude. The peak g_N change is at 88.4°E, 3.45°N about $-5.7 \pm 0.7 \mu\text{Gal}$ (Fig. S4a), slightly larger to the model prediction at the same location, $-3.7 \mu\text{Gal}$.

As discussed above, three products are all carried out to solve for the source parameters (Table S4) with centroid location fixed at GCMT solution. The CMT parameters agree amazingly well within these three products, especially for strike angle. The rake angle also has the small variation of only 1–2°, while a slightly larger divergence for moment and dip angle are shown with the smaller value given by OSU product. The solved M_0 ($10.13 \times 10^{21} \text{ Nm}$) from CSR RL05 product, the cumulative moment for both the mainshock and the aftershock, is close to the other published values. The M_0 is slightly smaller than the cumulative M_0 by GCMT solution ($12.03 \times 10^{21} \text{ Nm}$), USGS CMT solution ($10.7 \times 10^{21} \text{ Nm}$, http://earthquake.usgs.gov/earthquakes/eqinthenews/2012/usc000905e/neic_c000905e_cmt.php), and the published moment of the cumulative slip model ($16.79 \times 10^{21} \text{ Nm}$) by Yue et al. (2012). Our dip angle is also consistent with the dip angle given by other solutions, just about 4–5° smaller. As shown in Table 1 right, the correlation between dip and moment is about zero for this vertical strike-slip source, indicating the independence of the estimated dip angle and moment.

The rupture process of these intraplate earthquakes over the diffuse deformation zone is very complicated, and it raises speculations on whether it is dominated by east–west right-lateral slips (Meng et al., 2012; Yadav et al., 2013; Yue et al., 2012) or meridian-aligned left-lateral slips (Delescluse et al., 2012; Shao et al., 2012). Numerous preliminary results characterize the fault as a meridian-aligned left-lateral strike-slip (Shao et al., 2012). Nevertheless, the back projection source imaging from seismic data shows that the rupture of faults is dominated by east–west right-lateral slip (Meng et al., 2012; Yue et al., 2012). The east–west right-lateral slip model is further validated by the consistency with the remote GPS displacements (Yadav et al., 2013). Coherent with the fault plane by Yue et al. (2012), the GRACE-solved CMT also co-

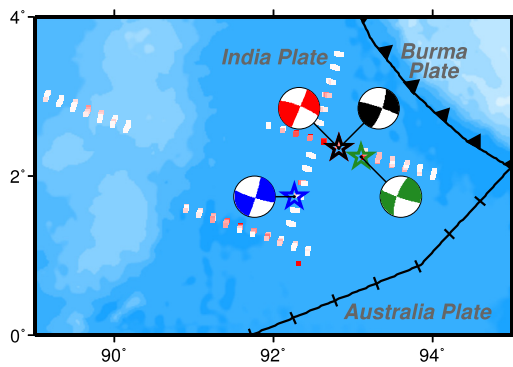


Fig. 8. Comparison of centroid moment tensor solutions for the 2012 Indian Ocean earthquakes. The white/red dot is the fault patches projected to the Earth's surface for the cumulative slip model by Yue et al. (2012) for mainshock and GCMT solution for aftershock, with its CMT located at the blue star and represented by the blue beach ball. Red beach ball is CMT solution from GRACE CSR RLO5 data, fixed at the GCMT location (black star). Other markings are the same as in Fig. 4. (For interpretation of the references to color in this figure legend, the reader is referred to the web version of this article.)

incides with an east–west right-lateral strike slip with strike angle as 292° . The reason why the strike angle by GRACE and GCMT solution is about 180° larger than that by Yue et al. (2012) and USGS CMT solution is that, for this nearly vertical strike-slip source, the dip direction is almost vertical and it is slightly tilted toward north for the former solutions and toward south for the latter as shown in Fig. 8. Taking into consideration of this 180° difference, GRACE-solved slip direction is amazingly consistent with the slip azimuth by other data, only $1\text{--}2^\circ$ different from the GCMT and USGS CMT solutions and 5° different from the cumulative model. For this vertical strike-slip earthquakes, the correlation (Table 1 right) between strike and rake angle is significantly reduced.

4.5. The 2007 Bengkulu earthquake

The 12 September 2007 Bengkulu (M_w 8.5) earthquake occurred off the west coast of Bengkulu, Indonesia (Konca et al., 2008; Gusman et al., 2010). It ruptured the plate interface at the Sumatra subduction zone where the Australia plate subducts beneath the Sunda plate, with the strike angle parallel to the Sunda trench. The relatively small seismic moment of this event renders it to be one of the ‘small’ earthquakes detectable by GRACE data (Tanaka et al., 2015). Same as for the 2012 Indian Ocean earthquakes, to crosscheck the reliability of the coseismic signal, three products for GRACE data are used to estimate the gravity and gravity gradient change corresponding to this 2007 Bengkulu earthquake. All solutions are truncated to degree 40 based on the localized spectral analysis (Fig. S5), as well as additional comparison in spatial domain. The RMS values of the model-data misfit for g_N , T_{xx} , T_{xy} , T_{xz} show that OSU product seems to give the lowest noise level with the smallest RMS misfit, while GFZ RL05a product gives the worst model-data misfit. Considering the comparison of the residual RMS as well as the comparison in spatial domain, we choose to present the gravity and gravity gradient change from OSU GRACE data product.

The localized degree variance (Fig. S5) shows that the difference between the GRACE-observed and model-predicted (Konca et al., 2008) g_N change is large for both the low degree part and high degree part, which indicates the GRACE noise level is relatively high for this comparatively small earthquake. The GRACE-derived T_{xx} , T_{xy} , T_{xz} changes agree with the model predictions for degree below 50 but with larger magnitude. With additional comparison in spatial domain by different maximum truncation degree, we choose to use the spherical harmonic coefficients below 40 to solve for fault mechanisms. As shown in Fig. 9, the spatial pat-

tern of the GRACE-derived north component of gravity and gravity gradient change still has good consistency with the model prediction. Nevertheless, the surrounding noise is relatively high for this small earthquake. For example, for the g_N change (Fig. 9a), there is an abnormal positive signal west coast of North Sumatra, which is absent in the model prediction (Fig. 9e). Similarly, over the same region, there is uncategorized negative signal for T_{xz} (Fig. 9d) change. Due to this large surrounding noise, it is not suggested to solve for the source location since the noise can be mistakenly treated as a signal and produce wrong source parameters.

All three products are used for the inversion of centroid moment tensor by fixing the centroid location at the GCMT solution. We can see that the divergence for three angles from the three products is large (Table S5), e.g. the difference is up to 11° for strike angle, 10° for dip angle, and 36° for rake angle. This larger variation for the solved source parameters, compared to the case for the 2012 Indian Ocean earthquakes, indicates again that the noise level from GRACE data is relatively high for this magnitude M_w 8.5 earthquake. Hence the large variation should be considered when interpret the GRACE-inverted source angles. Nevertheless, the self-consistency for the seismic moment is good from these three products of GRACE data.

For the seismic moment, GRACE-inverted M_0 from all three products is overall smaller than that from GCMT solution (6.71×10^{21} Nm) and that (4.47×10^{21} Nm) in Konca et al. (2008), with GFZ RL05a producing the closest M_0 (4.16×10^{21} Nm) to that in Konca et al. (2008). The GRACE-solved dip angle is overall larger than the published values, and the dip angle is 18° by CSR RLO5 product with the least discrepancy. During the three products, the OSU product produces the closest strike and rake angles with other results, e.g. rake angle (108°) is in-between the value given by GCMT and Konca et al. (2008) and it's only 2° larger than the rake angle by the joint inversion using tsunami waveforms and InSAR data in Gusman et al. (2010); but the strike angle is about 20° smaller causing the at least 16° smaller slip azimuth. On the other hand, the slip azimuth from CSR RLO5 and GFZ RL05a is consistent with the slip azimuth by GCMT and Konca et al. (2008), but the individual strike and rake angle are about $20\text{--}30^\circ$ smaller.

5. Conclusions

Advanced GRACE data processing procedure is developed in this paper using localized spectral analysis and using the north component of gravity and its corresponding gravity gradient changes. By establishing the observation model for north component of gravity and gravity gradient change as a linear function of the double-couple moment tensor, the point source parameters are resolved through the least-squares adjustment combined with the simulated annealing algorithm. The GRACE-inverted source parameters generally agree well with the slip models estimated using other data sets, including seismic, GPS, and their combination. While, their differences illustrate the additional and critical offshore constraint from GRACE data for improved estimates of source parameters, as compared to GPS/seismic data. For the 2004 Sumatra–Andaman and 2005 Nias earthquakes, GRACE data infer a shallower centroid depth (9.1 km), which may be explained by the closer-to-trench centroid and by the aseismic slip over the shallow region. For the 2011 Tohoku earthquake, GRACE-estimated centroid location and slip azimuth from two different GRACE data products and two different forward modeling are consistent with each other, demonstrating the coherence of the CSR RLO5 NMAX 60 and CSR RLO5 NMAX 96 products, as well as the coherence of the finite fault modeling and the point-source moment tensor modeling. The slip direction from GRACE data shows a clockwise rotation compared to the slip direction by GPS and seismic waves

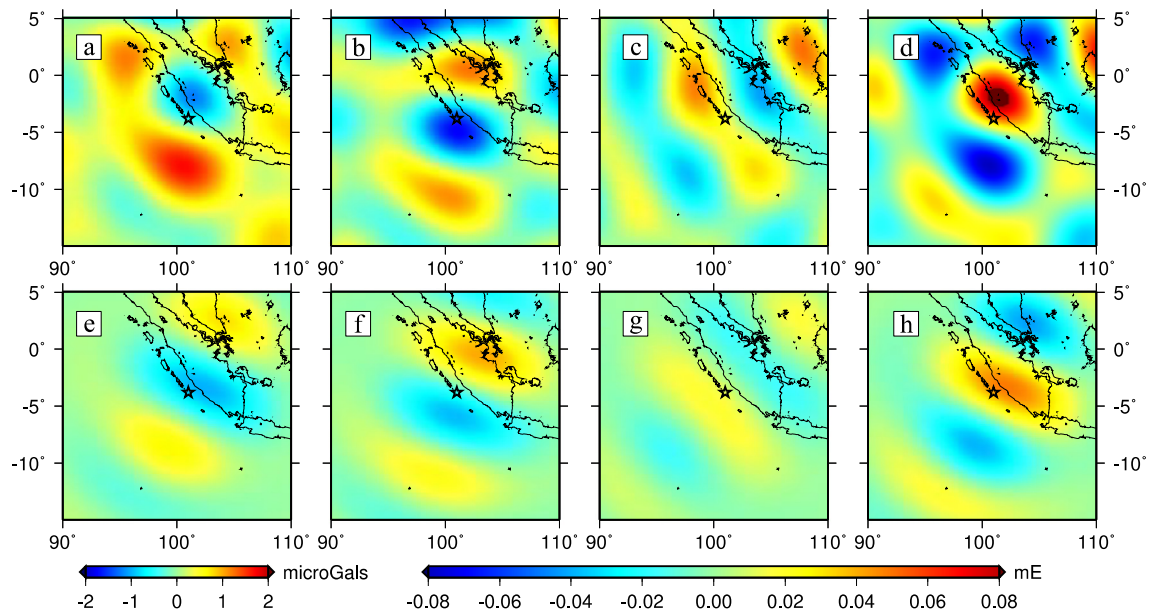


Fig. 9. Comparison of GRACE-produced and model-predicted gravity and gravity gradient change up to degree 40 from OSU product for the 2007 Bengkulu earthquake. (a)–(d): GRACE-observed g_N (a), T_{xx} (b), T_{xy} (c), T_{xz} (d) change, respectively. (e)–(h): model-predicted g_N (e), T_{xx} (f), T_{xy} (g), T_{xz} (h) change, respectively. The slip distribution model by Konca et al. (2008) is used to model the GRACE-commensurable gravity and gravity gradient change. The black star is the GCMT centroid (100.99°E, 3.78°S).

data, which is also observed by GOCE measurements (Fuchs et al., 2013). The GRACE-estimated dip directions are steeper than those from GPS/seismic data, about 18° steeper for the 2004 Sumatra–Andaman and 2005 Nias earthquakes, about 8° steeper for the 2010 Maule, Chile earthquake, and about 3–13° steeper for the 2007 Bengkulu earthquake. The larger dip angles for the 2004 Sumatra–Andaman earthquake and the 2010 Maule, Chile earthquake might be explained by the trade-off between the seismic moment and dip angle, as also indicated by their high correlations. For future studies, the question of how systematic errors from GRACE data and the errors in the forward modeling affect the inverted source parameters needs to be further investigated.

Acknowledgements

We acknowledge Frederik Simons, Princeton University, for providing his software on localized spectral analysis, and useful discussions. We thank Jeff Freymueller, University of Alaska, for his helpful suggestions and comments. We thank Shengji Wei, Han Yue, David Sandwell, and authors of the eQuake-RC, <http://equake-rc.info>, for providing various coseismic and postseismic slip models. We would like to thank Seiichi Miura who generously shares the velocity structure at the Japan Trench subduction zone. This research is supported by NASA's Earth and Space Science Fellowship (ESSF) Program (Grant NNX12A006H), by National Science Foundation (NSF) Division of Earth Sciences (Grant EAR-1013333), and by State Key Laboratory of Geodesy and Earth's Dynamics, IGG, CAS (No. Y309473047). GRACE data products are from NASA's PO-DAAC via Jet Propulsion Laboratory/California Institute of Technology (JPL), University of Texas Center for Space Research (CSR), and GeoForschungsZentrum Potsdam (GFZ). We thank Srinivas Bettadpur for providing high degree (up to degree 96) GRACE CSR RL05 data products. Some figures in this paper were generated using the Generic Mapping Tools (GMT) (Wessel and Smith, 1991). This work was supported in part by an allocation of computing time from the Ohio Supercomputer Center. We appreciate the constructive suggestions by Peter Shearer, Kosuke Heki, and an anonymous reviewer.

Appendix A. Supplementary material

Supplementary material related to this article can be found online at <http://dx.doi.org/10.1016/j.epsl.2016.03.025>.

References

- Banerjee, P., Pollitz, F., Bürgmann, R., 2005. Size and duration of the great 2004 Sumatra–Andaman earthquake from far-field static offsets. *Science* 308, 1769–1772.
- Bird, P., 2003. An updated digital model of plate boundaries. *Geochem. Geophys. Geosyst.* 4 (3), 1027. <http://dx.doi.org/10.1029/2001GC000252>.
- Cambiotti, G., Sabadini, R., 2012. A source model for the great 2011 Tohoku earthquake (Mw = 9.1) from inversion of GRACE gravity data. *Earth Planet. Sci. Lett.* 335–336, 72–79.
- Cambiotti, G., Sabadini, R., 2013. Gravitational seismology retrieving centroid-moment-tensor solution of the 2011 Tohoku earthquake. *J. Geophys. Res., Solid Earth* 118, 183–194. <http://dx.doi.org/10.1029/2012JB009555>.
- Chlieh, M., Avouac, J.P., Hjarleifsdottir, V., Song, T.A., Ji, C., Sieh, K., Sladen, A., Hebert, H., Prawirodirdjo, L., Bock, Y., Galetzka, J., 2007. Coseismic slip and afterslip of the great Mw 9.15 Sumatra–Andaman earthquake of 2004. *Bull. Seismol. Soc. Am.* 97 (1A), S152–S173.
- Dai, C., Shum, C.K., Wang, R., Wang, L., Guo, J., Shang, K., Tapley, B., 2014. Improved constraints on seismic source parameters of the 2011 Tohoku earthquake from GRACE gravity and gravity gradient changes. *Geophys. Res. Lett.* 41, 1929–1936. <http://dx.doi.org/10.1002/2013GL059178>.
- Delescluse, M., Chamot-Rooke, N., Cattin, R., Fleitout, L., Trubienko, O., Vigny, C., 2012. April 2012 intra-oceanic seismicity off Sumatra boosted by the Banda-Aceh megathrust. *Nature* 490, 240–244.
- Fuchs, M.J., Bouman, J., Broerse, T., Visser, P., Vermeersen, B., 2013. Observing coseismic gravity change from the Japan Tohoku-Oki 2011 earthquake with GOCE gravity gradiometry. *J. Geophys. Res., Solid Earth* 118, 5712–5721. <http://dx.doi.org/10.1002/jgrb.50381>.
- Geist, E.L., Titov, V.V., Arcas, D., Pollitz, F.F., Bilek, S.L., 2007. Implications of the 26 December 2004 Sumatra–Andaman earthquake on tsunami forecast and assessment models for great subduction zone earthquakes. *Bull. Seismol. Soc. Am.* 97 (1A), S249–S270.
- Guo, J.Y., Shang, K., Jekeli, C., Shum, C., 2015. On the energy integral formulation of gravitational potential differences from satellite-to-satellite tracking. *Celest. Mech. Dyn. Astron.* 121 (4), 415–429. <http://dx.doi.org/10.1007/s10569-015-9610-y>.
- Gusman, A.R., Tanioka, Y., Kobayashi, T., Latief, H., Pandoe, W., 2010. Slip distribution of the 2007 Bengkulu earthquake inferred from tsunami waveforms and InSAR data. *J. Geophys. Res.* 115, B12316. <http://dx.doi.org/10.1029/2010JB007565>.
- Han, S.-C., Riva, R., Sauber, J., Okal, E., 2013. Source parameter inversion for recent great earthquakes from a decade-long observation of global gravity fields. *J. Geophys. Res.* 118, 1240–1267. <http://dx.doi.org/10.1002/jgrb.50116>.

- Han, S.-C., Sauber, J., Luthcke, S., 2010. Regional gravity decrease after the 2010 Maule (Chile) earthquake indicates large-scale mass redistribution. *Geophys. Res. Lett.* 37, L23307. <http://dx.doi.org/10.1029/2010GL045449>.
- Han, S.C., Sauber, J., Pollitz, F., 2014. BROADSCALE POSTSEISMIC GRAVITY CHANGE FOLLOWING THE 2011 TOHOKU-OKI EARTHQUAKE AND IMPLICATION FOR DEFORMATION BY VISCOELASTIC RELAXATION AND AFTERSLIP. *Geophys. Res. Lett.* 41 (16), 5797–5805.
- Han, S.-C., Sauber, J., Riva, R., 2011. Contribution of satellite gravimetry to understanding seismic source processes of the 2011 Tohoku-Oki earthquake. *Geophys. Res. Lett.* 38, L24312. <http://dx.doi.org/10.1029/2011GL049975>.
- Han, S.-C., Shum, C., Bevis, M., Ji, C., Kuo, C., 2006. Crustal dilatation observed by GRACE after the 2004 Sumatra–Andaman earthquake. *Science* 313 (5787), 658–661.
- Hayes, G., 2010. Finite fault model, updated results of the Feb. 27, 2010 Mw 8.8 Maule, Chile earthquake. Available at: http://earthquake.usgs.gov/earthquakes/eqinthenews/2010/us2010fan/finite_fault.php (last accessed January 12 2015).
- Hayes, G.P., Wald, D.J., Johnson, R.L., 2012. Slab1.0: a three-dimensional model of global subduction zone geometries. *J. Geophys. Res.* 117, B01302. <http://dx.doi.org/10.1029/2011JB008524>.
- Heki, K., Matsuo, K., 2010. Coseismic gravity changes of the 2010 earthquake in central Chile from satellite gravimetry. *Geophys. Res. Lett.* 37, L24306. <http://dx.doi.org/10.1029/2010GL045335>.
- Kirkpatrick, S., Gelatt Jr., C.D., Vecchi, M.P., 1983. Optimization by simulated annealing. *Science* 220, 671–680. <http://dx.doi.org/10.1126/science.220.4598.671>.
- Konca, A.O., Avouac, J.-P., Sladen, A., Meltzner, A.J., Sieh, K., Fang, P., Li, Z., Galetzka, J., Genrich, J., Chlieh, M., Natawidjaja, D.H., Bock, Y., Fielding, E., Ji, C., Helmberger, D.V., 2008. Partial rupture of a locked patch of the Sumatra megathrust during the 2007 earthquake sequence. *Nature* 456, 631–635. <http://dx.doi.org/10.1038/nature07572>.
- Konca, Ozgun, A., Hjørleifsdóttir, V., Song, T.A., Avouac, J.P., Helmberger, D.V., Ji, C., Sieh, K., Briggs, R., Meltzner, A., 2007. Rupture kinematics of the 2005, Mw 8.6, Nias–Simeulue earthquake from the joint inversion of seismic and geodetic data. *Bull. Seismol. Soc. Am.* 97 (1A), S307–S322. <http://dx.doi.org/10.1785/0120050632>.
- Lay, T., Ammon, C.J., Kanamori, H., Koper, K.D., Sufri, O., Hutko, A.R., 2010. Teleseismic inversion for rupture process of the 27 February 2010 Chile (Mw 8.8) earthquake. *Geophys. Res. Lett.* 37, L13301. <http://dx.doi.org/10.1029/2010GL043379>.
- Lay, T., Ammon, C., Kanamori, H., Xue, L., Kim, M., 2011. Possible large near-trench slip during the 2011 Mw 9.0 off the Pacific coast of Tohoku Earthquake. *Earth Planets Space* 63, 687–692.
- Lay, T., Kanamori, H., Ammon, C.J., Koper, K.D., Hutko, A.R., Ye, L., Yue, H., Rushing, T.M., 2012. Depth-varying rupture properties of subduction zone megathrust faults. *J. Geophys. Res.* 117, B04311. <http://dx.doi.org/10.1029/2011JB009133>.
- Lay, T., Kanamori, H., Ammon, C.J., Nettles, M., Ward, S.N., Aster, R.C., Beck, S.L., Bilek, S.L., Brudzinski, M.R., Butler, R., DeShon, H.R., Ekstrom, G., Satake, K., Sipkin, S., 2005. The great Sumatra–Andaman earthquake of 26 December 2004. *Science* 308, 1127–1133.
- Li, J., Shen, W.B., 2011. Investigation of the co-seismic gravity field variations caused by the 2004 Sumatra–Andaman earthquake using monthly GRACE data. *J. Earth Sci.* 22 (2), 280–291.
- Li, Jin, Shen, W.B., 2015. Monthly GRACE detection of coseismic gravity change associated with 2011 Tohoku-Oki earthquake using northern gradient approach. *Earth Planets Space* 67, 1.
- Matsuo, K., Heki, K., 2011. Coseismic gravity changes of the 2011 Tohoku-Oki earthquake from satellite gravimetry. *Geophys. Res. Lett.* 38, L00G12. <http://dx.doi.org/10.1029/2011GL049018>.
- Meng, L., Ampuero, J.-P., Stock, J., Duputel, Z., Luo, Y., Tsai, V.C., 2012. Earthquake in a maze: compressional rupture branching during the 2012 Mw 8.6 Sumatra earthquake. *Science* 337, 724–726.
- Miura, S., Takahashi, N., Nakanishi, A., Tsuru, T., Kodaira, S., Kaneda, Y., 2005. Structural characteristics off Miyagi forearc region, the Japan Trench seismogenic zone, deduced from a wide-angle reflection and refraction study. *Tectonophysics* 407 (3), 165–188.
- Ozawa, S., Nishimura, T., Suito, H., Kobayashi, T., Tobita, M., Imakiire, T., 2011. Coseismic and postseismic slip of the 2011 magnitude-9 Tohoku-Oki earthquake. *Nature* 475, 373–376. <http://dx.doi.org/10.1038/nature10227>.
- Panet, I., Pollitz, F.F., Mikhailov, V., Diament, M., Banerjee, P., Grijalva, K., 2010. Upper mantle rheology from GRACE and GPS postseismic deformation after the 2004 Sumatra–Andaman earthquake. *Geochem. Geophys. Geosyst.* 11, Q06008. <http://dx.doi.org/10.1029/2009GC002905>.
- Park, J., Song, T.R.A., Tromp, J., Okal, E., Stein, S., Roullet, G., Clevede, E., Laske, G., Kanamori, H., Davis, P., Berger, J., Braitenberg, C., Van Camp, M., Lei, X., Sun, H.P., Xu, H.Z., Rosat, S., 2005. Earth's free oscillations excited by the 26 December 2004 Sumatra–Andaman earthquake. *Science* 308, 1139–1144.
- Poisson, B., Oliveros, C., Pedreros, R., 2011. Is there a best source model of the Sumatra 2004 earthquake for simulating the consecutive tsunami? *Geophys. J. Int.* 185, 1365–1378.
- Pollitz, F.F., et al., 2011. Coseismic slip distribution of the February 27, 2010 Mw 8.8 Maule, Chile earthquake. *Geophys. Res. Lett.* 38, L09309. <http://dx.doi.org/10.1029/2011GL047065>.
- Rhie, J., Dreger, D., Bürgmann, R., Romanowicz, B., 2007. Slip of the 2004 Sumatra–Andaman earthquake from joint inversion of long period global seismic waveforms and GPS static offsets. *Bull. Seismol. Soc. Am.* 97 (1A), S115–S127.
- Shang, K., Guo, J.Y., Shum, C.K., Dai, C., Luo, J., 2015. GRACE time-variable gravity field recovery using an improved energy balance approach. *Geophys. J. Int.* 203 (3), 1773–1786. <http://dx.doi.org/10.1093/gji/ggv392>.
- Shao, G., Li, X., Ji, C., 2012. Preliminary result of the Apr 11, 2012 Mw 8.64 Sumatra earthquake. http://www.geol.ucsb.edu/faculty/ji/big_earthquakes/2012/04/10/sumatra.html (last accessed January 13, 2015).
- Simons, F., Dahlen, F., Wiecek, M., 2006. Spatiospectral concentration on a sphere. *SIAM Rev.* 48 (3), 504–536. <http://dx.doi.org/10.1137/S0036144504445765>.
- Tanaka, Y., Heki, K., 2014. Long- and short-term postseismic gravity changes of megathrust earthquakes from satellite gravimetry. *Geophys. Res. Lett.* 41, 5451–5456. <http://dx.doi.org/10.1002/2014GL060559>.
- Tanaka, Y., Heki, K., Matsuo, K., Shestakov, N.V., 2015. Crustal subsidence observed by GRACE after the 2013 Okhotsk deep-focus earthquake. *Geophys. Res. Lett.* 42, 3204–3209. <http://dx.doi.org/10.1002/2015GL063838>.
- Tanioka, Y., Satake, K., 1996. Tsunami generation by horizontal displacement of ocean bottom. *Geophys. Res. Lett.* 23, 891–894.
- Tapley, B.D., Bettadpur, S., Ries, J.C., Thompson, P.F., Watkins, M.M., 2004. GRACE measurements of mass variability in the Earth system. *Science* 305, 503–505.
- Vigny, C., et al., 2011. The 2010 Mw 8.8 Maule megathrust earthquake of central Chile, monitored by GPS. *Science* 332, 1417–1421. <http://dx.doi.org/10.1126/science.1204132>.
- Wang, L., Shum, C., Simons, F., Tassara, A., Erkan, K., Jekeli, C., Braun, A., Kuo, C., Lee, H., Yuan, D., 2012a. Coseismic slip of the 2010 Mw 8.8 Great Maule, Chile, earthquake quantified by the inversion of GRACE observations. *Earth Planet. Sci. Lett.* 335–336, 167–179.
- Wang, L., Shum, C., Simons, F., Tapley, B., Dai, C., 2012b. Coseismic and post-seismic deformation of the 2011 Tohoku-Oki earthquake constrained by GRACE gravimetry. *Geophys. Res. Lett.* 39, L07301. <http://dx.doi.org/10.1029/2012GL051104>.
- Wang, L., Shum, C., Jekeli, C., 2012c. Gravitational gradient changes following the 2004 December 26 Sumatra–Andaman Earthquake inferred from GRACE. *Geophys. J. Int.* 191 (3), 1109–1118. <http://dx.doi.org/10.1111/j.1365-246X.2012.05674.x>.
- Wang, R., Parolai, S., Ge, M., Ji, M., Walter, T.R., Zschau, J., 2013. The 2011 Mw 9.0 Tohoku-Oki earthquake: comparison of GPS and strong-motion data. *Bull. Seismol. Soc. Am.* 103 (2B), 1336–1347. <http://dx.doi.org/10.1785/0120110264>.
- Wei, Shengji, Graves, R., Helmberger, D., Avouac, J.P., Jiang, J., 2012. Sources of shaking and flooding during the Tohoku-Oki earthquake: a mixture of rupture styles. *Earth Planet. Sci. Lett.* 333–334, 91–100.
- Wessel, P., Smith, W.H.F., 1991. Free software helps map and display data. *Eos Trans. AGU* 72 (41), 441. <http://dx.doi.org/10.1029/90EO00319>.
- Wiecek, M.A., Simons, F.J., 2005. Localized spectral analysis on the sphere. *Geophys. J. Int.* 162, 655–675.
- Yadav, R.K., Kundu, B., Gahalaut, K., Catherine, J., Gahalaut, V.K., Ambikapathy, A., Naidu, M.S., 2013. Coseismic offsets due to the 11 April 2012 Indian Ocean earthquakes (Mw 8.6 and 8.2) derived from GPS measurements. *Geophys. Res. Lett.* 40, 3389–3393. <http://dx.doi.org/10.1002/grl.50601>.
- Yue, H., Lay, T., Koper, K., 2012. En échelon and orthogonal fault ruptures of the 11 April 2012 great intraplate earthquakes. *Nature* 490, 245–249. <http://dx.doi.org/10.1038/nature11492>.